pH determines the energetic efficiency of the cyanobacterial CO_2 concentrating mechanism

Niall M. Mangan[a,1], Avi Flamholz[b,1], Rachel D. Hood[b], Ron Milo[c], and David F. Savage[b,d,2]

[a]Department of Applied Mathematics, University of Washington, Seattle, WA 98195; [b]Department of Molecular and Cell Biology, University of California, Berkeley, CA 94720; [c]Department of Plant and Environmental Sciences, Weizmann Institute of Science, Rehovot 76100, Israel; and [d]Department of Chemistry, University of California, Berkeley, CA 94720

Edited by George H. Lorimer, University of Maryland, College Park, MD, and approved July 11, 2016 (received for review December 22, 2015)

Many carbon-fixing bacteria rely on a CO_2 concentrating mechanism (CCM) to elevate the CO_2 concentration around the carboxylating enzyme ribulose bisphosphate carboxylase/oxygenase (RuBisCO). The CCM is postulated to simultaneously enhance the rate of carboxylation and minimize oxygenation, a competitive reaction with O_2 also catalyzed by RuBisCO. To achieve this effect, the CCM combines two features: active transport of inorganic carbon into the cell and colocalization of carbonic anhydrase and RuBisCO inside proteinaceous microcompartments called carboxysomes. Understanding the significance of the various CCM components requires reconciling biochemical intuition with a quantitative description of the system. To this end, we have developed a mathematical model of the CCM to analyze its energetic costs and the inherent intertwining of physiology and pH. We find that intracellular pH greatly affects the cost of inorganic carbon accumulation. At low pH the inorganic carbon pool contains more of the highly cell-permeable H_2CO_3, necessitating a substantial expenditure of energy on transport to maintain internal inorganic carbon levels. An intracellular pH ≈8 reduces leakage, making the CCM significantly more energetically efficient. This pH prediction coincides well with our measurement of intracellular pH in a model cyanobacterium. We also demonstrate that CO_2 retention in the carboxysome is necessary, whereas selective uptake of HCO_3^- into the carboxysome would not appreciably enhance energetic efficiency. Altogether, integration of pH produces a model that is quantitatively consistent with cyanobacterial physiology, emphasizing that pH cannot be neglected when describing biological systems interacting with inorganic carbon pools.

carbon fixation | RuBisCO | cyanobacteria | inorganic carbon | systems biology

Cyanobacteria and many other autotrophs use a CO_2 concentrating mechanism (CCM) to increase the cellular pool of inorganic carbon and facilitate the Calvin–Benson–Bassham (CBB) cycle (1). Specifically, the CCM functions to supply CO_2 to ribulose bisphosphate carboxylase/oxygenase (RuBisCO), the primary carboxylating enzyme of the CBB cycle. High levels of CO_2 are essential to cyanobacterial metabolism because RuBisCO has relatively slow carboxylation kinetics and is promiscuous, catalyzing an off-pathway reaction with O_2 called oxygenation (2–4).

RuBisCO oxygenation produces 2-phosphoglycolate (2PG), which is not part of the CBB cycle and must be recycled. Recycling 2PG through photorespiratory pathways is costly, consuming reduced carbon and energy resources (5, 6). The problem of RuBisCO's limited specificity is all the more pronounced because there is ≈20 times more O_2 than CO_2 in aqueous solutions equilibrated with present-day atmosphere (*SI Appendix*, Fig. S1). CCMs overcome these problems by concentrating CO_2 near RuBisCO, favorably increasing the ratio of CO_2 to O_2. High concentrations of CO_2 maximize the rate of carboxylation and competitively inhibit oxygenation. Indeed, it is widely thought that the evolution of CCMs served to ameliorate energetic costs associated with large photorespiratory fluxes in the present-day atmosphere (7).

Based on diverse experimental studies, a convincing model of the bacterial CCM has emerged (Fig. 1) wherein the CCM has two primary components: active accumulation of inorganic carbon (Ci) in the cytosol and organization of RuBisCO with carbonic anhydrase (CA) inside proteinaceous organelles called carboxysomes (8). Perturbations to either component disrupt the CCM and produce mutants that require elevated CO_2 for growth (9, 10). Two energetically activated transport mechanisms—HCO_3^- transport and facilitated uptake of CO_2—enable accumulation of bicarbonate (HCO_3^-) in the cytosol (8). HCO_3^- transport is generally coupled to Na^+ gradients or ATP hydrolysis and facilitated uptake is hypothesized to couple oxidation of NAD(P)H to unidirectional hydration of CO_2 (Fig. 1) (8). Accumulation of charged HCO_3^- is preferable to accumulation of CO_2 because HCO_3^- escapes much less readily through the cell membrane, as we discuss below. Together, these uptake systems generate a cytosolic HCO_3^- concentration >10 mM, which is ≈30 times the equilibrium concentration of HCO_3^- in water at neutral pH at 25 °C (*SI Appendix*, Fig. S1) (11).

Carboxysomes are icosahedral compartments approximately 100 nm in diameter and composed of a protein shell surrounding an enzyme-filled lumen (12). The carboxysome lumen is densely packed (>400 mg protein/mL) with about 2,000 RuBisCO and 100 CA active sites (12). Because CA activity is absent from the cytosol and the spontaneous dehydration of HCO_3^- to CO_2 is relatively slow (13), HCO_3^- does not equilibrate with CO_2 in the cytosol (10). Rather, HCO_3^- enters the carboxysome where CA activity readily equilibrates it with CO_2 (10). Crucially, the carboxysome shell

Significance

Cyanobacteria are responsible for roughly 10% of global photosynthetic primary production of reduced carbon. Although cyanobacteria are incredibly diverse, all known species contain a complex protein system called the CO_2 concentrating mechanism (CCM), which enables rapid growth even in environments with extremely limited CO_2. The CCM enables cyanobacteria to accumulate HCO_3^- and convert this inorganic carbon pool to utilizable CO_2. We demonstrate here that a quantitative description of the CCM must include the effect of pH on the abundance of HCO_3^- and H_2CO_3. This pH-dependent description is consistent with cyanobacterial physiology. Furthermore, the model predicts that alkaline cytosolic pH reduces the energetic cost of the CCM, consistent with pH measurements of photosynthesizing cyanobacteria.

Author contributions: N.M.M., A.F., R.D.H., R.M., and D.F.S. designed research; N.M.M., A.F., R.D.H., R.M., and D.F.S. performed research; N.M.M. and A.F. contributed new reagents/analytic tools; N.M.M., A.F., R.D.H., R.M., and D.F.S. analyzed data; and N.M.M., A.F., R.M., and D.F.S. wrote the paper.

The authors declare no conflict of interest.

This article is a PNAS Direct Submission.

[1]N.M.M. and A.F. contributed equally to this work.

[2]To whom correspondence should be addressed. Email: savage@berkeley.edu.

This article contains supporting information online at www.pnas.org/lookup/suppl/doi:10.1073/pnas.1525145113/-/DCSupplemental.

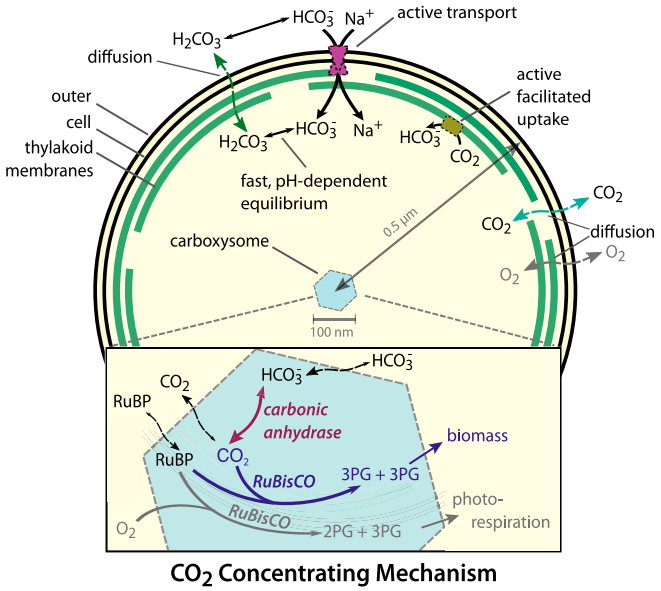

Fig. 1. Schematic of the generally accepted model of the cyanobacterial CCM. The cyanobacterial CCM concentrates HCO_3^- in the cytosol via two classes of uptake systems: transporters and facilitated uptake systems. We focus on Na^+-activated transporters, which transport one Na^+ with each HCO_3^-. Facilitated uptake of CO_2 is catalyzed by proteins on the thylakoid membrane and is thought to couple NAD(P)H oxidation to the vectorial conversion of CO_2 into HCO_3^-. Roughly 250 RuBisCOs (2,000 active sites) and 100 CAs are localized to the carboxysome. HCO_3^- concentrated in the cytosol enters the carboxysome, where it is converted to a high CO_2 concentration by CA activity. This elevated CO_2 concentration increases the rate of RuBisCO carboxylation and competitively inhibits oxygenation, increasing the overall efficiency of carbon fixation. For parameter values and model details see *SI Appendix*. References for each model component are given in the main text. 3PG, 3-phosphoglycerate.

must slow the diffusive loss of CO_2 so that CA activity produces a locally elevated carboxysomal CO_2 concentration (9). At sufficiently high CO_2 concentrations, RuBisCO is saturated, oxygenation is inhibited, and carboxylation proceeds at the maximum rate (1).

To define the regimes wherein the cyanobacterial CCM leads to efficient carbon fixation, we previously developed a reaction-diffusion model of the CCM (14). Even when presented with very low extracellular CO_2 concentrations (i.e., very high relative O_2 concentrations), the modeled CCM can saturate RuBisCO and drastically reduce oxygenation (14). Surprisingly, the model suggested that the CCM does not require selective uptake of HCO_3^- into the carboxysome, selective retention of CO_2 inside the compartment, or exclusion of O_2. Rather, a nonspecific permeability barrier at the carboxysome shell could give rise to CO_2-concentrating activity. These results built upon previous models (7, 15–17) and further explained how CCM activity, which makes cyanobacterial growth largely insensitive to the environmental concentration of Ci, could arise from its known protein components.

An unexplained observation of our previous work was substantial leakage of HCO_3^- across the cell membrane, with >99% of carbon import leaking out of the cell as HCO_3^- (14). Because HCO_3^- accumulation is energetically driven, large leakage fluxes consume substantial energy and require an implausible fraction (>50%) of the membrane surface for transporters (*SI Appendix*). Here, we identify the cell membrane permeability to HCO_3^- as a key parameter determining leakage. All previous models of the CCM tracked only HCO_3^-, implicitly ignoring other species of hydrated Ci (H_2CO_3, HCO_3^-, and CO_3^{2-}, which we collectively term H_{total}) and their contribution to cell permeability (14–19). This implicit assumption is at odds with biochemical intuition that charge is a major determinant of membrane permeability (20). Indeed, the often-cited permeability coefficient of $\approx 3 \times 10^{-4}$ cm/s is representative of the uncharged H_2CO_3 but three to four orders of magnitude too high for HCO_3^- and CO_3^{2-} (*SI Appendix*) (21, 22). A recent model of the minimal CCM of *Prochlorococcus* MED4 made the inverse assumption: that the cell membrane is negligibly permeable to HCO_3^-, implicitly ignoring the rapid interconversion of HCO_3^- with the uncharged and highly permeable H_2CO_3 (23).

To reconcile these varying treatments and conduct a careful accounting of Ci species, we take advantage of pH as a key physiological parameter governing the composition of the Ci pool. The relative concentration of species in H_{total} (H_2CO_3, HCO_3^-, and CO_3^{2-}) depends strongly on pH (*SI Appendix*, Fig. S1). Because these species differ in their net charge, pH will influence the rate of Ci leakage from the cell and the energetic costs associated with carbon accumulation. Because RuBisCO and CA activities are pH-dependent, the pH will also affect enzymatic rates inside the carboxysome. We have integrated these effects into our previous analytical and numerical models of the CCM (14) to produce a "pH-aware" model of the CCM, which is described in mathematical detail in *SI Appendix*.

The pH-aware model is now consistent with cyanobacterial physiology in a number of important ways. In optimal conditions, the model produces absolute fluxes that are similar to measured values and consistent with cyanobacterial growth rates. Unlike in previous models, these fluxes can be supported by transporters occupying a very small fraction of membrane surface area (<1%), leaving space for the essential biochemistry of transport, photosynthesis, and chemiosmosis (*SI Appendix*). Finally, characteristic differences in the Ci transport modalities used by oceanic and freshwater cyanobacteria can be explained through the pH-aware model by the characteristic pH and salinity differences between ocean and freshwater (*SI Appendix*). Given this broad consistency with cyanobacterial physiology and genetics, the pH-aware model can also be used to examine open questions related to the CCM.

Our updated, pH-aware model also enables us to test the hypothesis that the CCM reduces the energetic costs associated with fixing carbon. We calculate the effect of pH on the energetic cost of carbon fixation, carbon concentration, and photorespiration. According to our calculation, the CCM requires considerably less energy than implied by our previous model (*SI Appendix*). We further demonstrate that a selective carboxysome that prefers to take up HCO_3^- and retain CO_2 is not required to produce an energy-efficient CCM. Rather, a low absolute permeability to CO_2 is the crucial characteristic of an energy-efficient carboxysome. Moreover, the pH-aware model predicts an intracellular pH range that optimizes CCM efficiency in cyanobacteria actively fixing carbon. We validate this prediction by measuring the intracellular pH in live cyanobacterial cells (*Synechococcus elongatus* PCC 7942). Thus, the CCM offers another example where the properties of complex systems central to bacterial growth are well-explained by the principle of energetic cost minimization (24–26), in this case explaining the remodeling of cytosolic pH and transport modalities to minimize the cost of Ci accumulation for the CCM.

Results

The Effect of pH on the Permeability of Ci to the Cell Membrane. All cells regulate their cytosolic pH due to the inherent pH dependence of biochemical reactions (27). However, cytosolic pH varies substantially between organisms and growth conditions (28, 29). Here, we use a mathematical model to examine how the cyanobacterial CCM functions over a range of cytosolic pH values. We include the effect of pH on the permeability of the cell membrane to constituents of the Ci pool and on the enzymatic activities located within the carboxysome.

The equilibrium composition of the Ci pool (CO_2, H_2CO_3, HCO_3^-, and CO_3^{2-}) is highly pH-dependent (*SI Appendix*, Fig. S1). Whether these species reach equilibrium with each other, however, depends on how the rate of uncatalyzed interconversion compares to the rates of other processes (e.g., transport and enzymatic catalysis) that produce and consume specific species. The spontaneous dehydration of H_{total} to CO_2 [$T_{1/2} > 10$ s (13)] is much slower than diffusion and transport, and so the CCM can maintain H_{total} out of equilibrium with CO_2 in the cytosol (10). Equilibration between HCO_3^-, H_2CO_3, and CO_3^{2-} within the H_{total} pool is, however, extremely fast [$T_{1/2} < 1$ μs (30)]. As such, the dominant species among HCO_3^-, H_2CO_3, and CO_3^{2-} will be determined by the pH, and so the contribution of each species to the cell permeability of H_{total} must be examined individually.

Due to the energetic penalty associated with the passage of charge into the membrane, small, charged molecules typically have membrane permeability coefficients 10^4 to 10^5 times smaller than uncharged molecules of comparable size (20). Consequently, HCO_3^- and CO_3^{2-} are dramatically less cell-permeable than the uncharged H_2CO_3. In addition to having a low membrane permeability, CO_3^{2-} contributes negligibly (<5%) to the H_{total} pool below pH 9 and can be neglected (*SI Appendix*). As such, H_2CO_3 can be treated as a monoprotic acid equilibrating quickly with HCO_3^-. The primary literature on the permeability of small molecules gives permeability coefficients of $\approx 10^{-3}$ cm/s for H_2CO_3 and $\approx 10^{-7}$ cm/s for HCO_3^- (21, 22).

Given these values, we assume $k_m^{H_2CO_3} \ll k_m^{HCO_3^-}$ and derive that the rate of H_{total} diffusion across the membrane is dominated by the diffusion of uncharged H_2CO_3

$$\text{diffusive } H_{total} \text{ flux} = k_m^{H_2CO_3}\Delta H_2CO_3 + k_m^{HCO_3^-}\Delta HCO_3^- \approx k_m^{H_2CO_3}\Delta H_2CO_3.$$

Here, ΔH_2CO_3 and ΔHCO_3^- are the concentration differences of H_2CO_3 and HCO_3^- across the cell membrane (see *SI Appendix* for derivation). To a first approximation, H_2CO_3 is the only species of H_{total} that will cross the cell membrane diffusively at an appreciable rate, regardless of the relative concentrations of H_2CO_3 and HCO_3^-.

The above equation describes the diffusion of H_{total} into the cell as a function of the H_2CO_3 concentration gradient. However, the CCM model tracks HCO_3^- and not H_2CO_3 because HCO_3^- is the substrate of CA. To integrate this equation into the CCM model, therefore, we assume fast equilibrium of the H_{total} pool and calculate the equilibrium ratio $[HCO_3^-]/[H_2CO_3] = 10^{pH-pK_1}$ to determine ΔH_2CO_3 across the cell membrane. Because the concentration and composition of H_{total} may differ markedly across the cell membrane (due to differences in pH, ionic strength, and the action of Ci transporters), this substitution yields separate terms for the inward (first term) and outward (second term) diffusional velocities

$$\text{diffusive } HCO_3^- \text{ flux} = \left([HCO_3^-]_{out}\, k_m^{H_2CO_3}\, 10^{(pK_1 - pH_{out})} - [HCO_3^-]_{cytosol}\, k_m^{H_2CO_3}\, 10^{(pK_1 - pH_{cytosol})} \right).$$

Here, $k_m^{H_2CO_3} = 3 \times 10^{-3}$ cm/s is the velocity of H_2CO_3 permeation and $10^{(pK_1 - pH)}$ is the ratio of H_2CO_3 to HCO_3^- as a function of the pH and the first pK_a of H_2CO_3 ($pK_1 \approx 3.2$) (22, 31). This equation holds across the entire pH range considered here ($6.5 \le pH \le 9$; see *SI Appendix* for full derivation). If the cytosolic and extracellular pH are equal, the pH-dependent velocity of HCO_3^- membrane permeation equals $k_m^{H_2CO_3}\, 10^{(pK_1 - pH)}$, recovering a functional form equivalent to the previous model. At pH 7, this equation yields a velocity of $\approx 5 \times 10^{-7}$ cm/s, 1,000-fold smaller than the commonly used value of 3×10^{-4} cm/s (32, 33). Indeed, this higher effective velocity implies an implausible cytosolic pH of about 4 (*SI Appendix*).

Functional Form of the pH-Aware CCM Model. The pH-aware CCM model is a system of coupled reaction-diffusion differential equations in spherical coordinates. The equations describe the entry of Ci into the cell and the carboxysome as well as diffusion and the chemical reactions within the carboxysome. This system can be solved both numerically and analytically at steady state (14). We write the fluxes for CO_2, C, and HCO_3^-, H, at the cell membrane, $r = R_b$, as

$$D\frac{\partial C}{\partial r} = -\alpha C_{cytosol} + k_m^C\left(C_{out} - C_{cytosol}\right)$$

$$D\frac{\partial H}{\partial r} = j_c H_{out} + \alpha C_{cytosol} + \left([HCO_3^-]_{out}\, k_m^{H_2CO_3}\, 10^{(pK_1 - pH_{out})} - [HCO_3^-]_{cytosol}\, k_m^{H_2CO_3}\, 10^{(pK_1 - pH_{cytosol})} \right).$$

Here D is the diffusion constant for small molecules in water (10^{-5} cm^2/s), j_c is the velocity of active HCO_3^- transport, α is the velocity of CO_2 to HCO_3^- conversion, and k_m^C and $k_m^{H_2CO_3}$ are the permeability of the cell membrane to CO_2 and H_2CO_3, respectively. k_m^C is set to 0.3 cm/s and $k_m^{H_2CO_3} = 3 \times 10^{-3}$ cm/s as described above.

As previously discussed, the spontaneous dehydration of HCO_3^- is slow, so we assume no relevant chemical reactions in the cytosol (Fig. 1). We evaluate this assumption through a consistency check on the resulting model concentrations and fluxes and find it to be reasonable (*SI Appendix*). Therefore, diffusion sets the steady-state concentrations of CO_2 and HCO_3^- in the cytosol via $\nabla^2 C = 0$, $\nabla^2 H = 0$, where ∇^2 is the second derivative in spherical coordinates. Assuming the same carboxysome permeability, k_c, for both CO_2 and HCO_3^-, diffusive leakage at the carboxysome shell is expressed as

$$D\frac{\partial C}{\partial r} = k_c\left(C_{cytosol} - C_{carboxysome}\right)$$

$$D\frac{\partial H}{\partial r} = k_c\left(H_{cytosol} - H_{carboxysome}\right)$$

at r = R_c, the boundary of the carboxysome. The pH-aware model can also be used to consider differential carboxysome permeability to CO_2 and HCO_3^-, as described in *Discussion* and *SI Appendix*. Inside the carboxysome, the model considers diffusion of substrates as well as CA (R_{CA}) and RuBisCO (R_{Rub}) activities. The balance of enzymatic and diffusive rates set the steady-state concentrations of CO_2 and HCO_3^- in the carboxysome as

$$D\nabla^2 C + R_{CA} - R_{Rub} = 0$$

$$D\nabla^2 H - R_{CA} = 0,$$

where the enzymatic rates R_{CA} and R_{Rub} are depend on pH in the manner described below.

The Effect of pH on Enzymatic Activity in the Carboxysome. The enzymatic mechanisms of RuBisCO and CA are inherently pH-dependent (34), and so it is critical to include the pH dependence of these enzymes in describing the pH dependence of the CCM. The carboxysomal CA is an efficient enzyme, well described by reversible Michaelis–Menten kinetics, with a dehydration $k_{cat} \approx 5 \times 10^5$ s^{-1} (35). When the intrashellular CA is saturated,

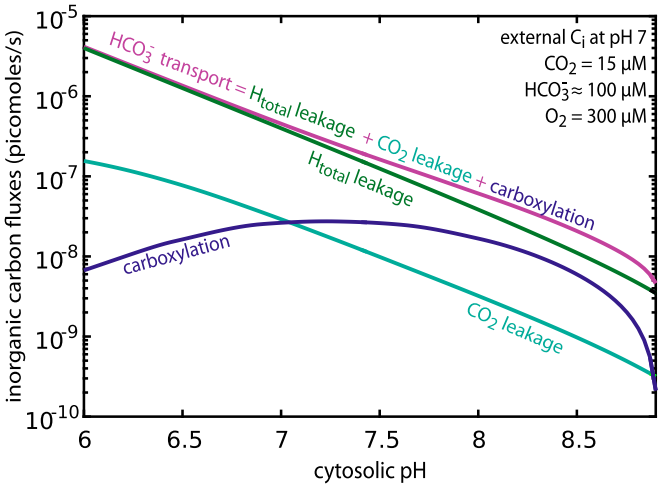

Fig. 2. Increased cytosolic pH reduces Ci fluxes required to achieve efficient CO_2 fixation. Ci fluxes are plotted as a function of pH. As carbon is conserved, the HCO_3^- transport flux (purple) equals the sum of H_{total} leakage (green), CO_2 leakage (teal), and carboxylation (blue). RuBisCO achieves a maximum carboxylation rate near pH 7.5. Carboxysome permeability was set to 3×10^{-5} cm/s and HCO_3^- transport rate was set to yield 30 mM cytosolic HCO_3^- at each pH. The extracellular Ci pool was assumed to be in equilibrium with the external pH, which was fixed at 7 for this analysis. These fluxes neglect the uncatalyzed dehydration of HCO_3^-, which would act to increase CO_2 leakage. Compensating for increased leakage would require a small increase in HCO_3^- transport (*SI Appendix*).

increased HCO_3^- transport has no effect on the carboxysomal CO_2 concentration. As a result, saturated CA implies that HCO_3^- uptake could be lower without affecting the carboxylation rate (14). Therefore, efficient CCM function occurs, in part, when CA is not saturated. Because CA is a fast enzyme with ≈100 active sites in the carboxysome, CO_2 and HCO_3^- are held in equilibrium within the carboxysome when CA is not saturated (*SI Appendix*). In this pseudoequilibrium condition, the ratio of CO_2 to HCO_3^- in the carboxysome is determined by the pH dependence of the reaction equilibrium constant $K_{eq}^{'}(pH) = [HCO_3^-]/[CO_2]$. We calculate the pH dependence of $K_{eq}^{'}$ from the Gibbs formation energies of the relevant species (27, 36). For reversible reactions such as the dehydration of bicarbonate, a modest change in the pH can have a large effect on $K_{eq}^{'}$—about 10-fold between pH 7 and 8 (*SI Appendix*).

RuBisCO activity also varies with pH, with the carboxylation k_{cat} reaching maximum near pH 7.5 (34). We describe the RuBisCO reaction with irreversible Michaelis–Menten kinetics and assume RuBisCO kinetic parameters measured at pH 7.8 for the *S. elongatus* PCC 6301 RuBisCO. The pH dependence of RuBisCO kinetics was modeled by rescaling the Michaelis–Menten kinetic constants by the pH dependence observed for the cyanobacterial RuBisCO from *Anabaena variabilis* (*SI Appendix*, Fig. S4).

A pH-Aware CCM Model. With the pH dependence of permeability and enzymatic activity integrated into the model, we asked a simple question: What is the role of cytosolic pH in shaping the flow of carbon through the CCM? To answer this question, we calculated the HCO_3^- transport flux required to achieve the measured ≈30 mM cytosolic HCO_3^- concentration (37–39) across a range of cytosolic pH values (Fig. 2). For this calculation, the carboxysome permeability was set to 3×10^{-5} cm/s (optimum for cytosolic pH 8; *SI Appendix*) and facilitated CO_2 uptake was set to zero for simplicity. The carboxysome permeability represents the velocity at which CO_2 and HCO_3^- traverse the carboxysome shell, including both transit of pores found in shell proteins and any "leakiness" of the shell itself. Carbon is conserved and so fluxes importing Ci into the cell (active HCO_3^- transport) must equal the sum of fluxes consuming Ci within the cell: H_{total} leakage, CO_2 leakage, and carboxylation. This conservation law is captured by the equation shown in Fig. 2.

Analyzing the pH dependence of carbon fluxes shows that CCM performance is expected to improve dramatically with increasing cytosolic pH (Fig. 2). Indeed, the amount of active transport required to maintain 30 mM cytosolic HCO_3^- decreases exponentially with increasing pH (i.e., linearly on a log scale). At pH 7 and below, more than 85% of the HCO_3^- influx leaks out of the cell. Above pH 7, CO_2 leakage and carboxylation fluxes contribute more prominently to the flux balance, with leakage representing ≈65% at pH 8. The log-linear relationship between pH and H_{total} leakage arises from the exponential (power-law) dependence of H_{total} permeability on pH described above. HCO_3^- transport fluxes also display a log-linear relationship with cytosolic pH (Fig. 2) and absolute transport rates at pH 8 are on the order of 10^{-7} pmol per cell per s, approaching the ≈10^{-8} pmol per cell per s uptake flux measured in the marine cyanobacterium *Prochlorococcus* MED4 (23).

In Fig. 2, the carboxylation rate declines above pH 7.5 because RuBisCO achieves maximal catalytic rate at that pH (34). At a cytosolic pH of 8 ≈30% of Ci uptake is ultimately fixed by RuBisCO, compared with ≈1% in the previous model. Economic operation of the CCM is strongly dependent on the cytosolic pH, with pH ≅8 curtailing diffusive loss of H_{total}. Although greatly reduced, loss of HCO_3^- (through H_2CO_3 leakage) remains a substantial flux and cannot be neglected even above pH 8. A full description of the model, including all kinetic parameters and pH dependencies, is given in *SI Appendix*.

The Energetic Cost of CO_2 Fixation. The pH-aware model can also be used to calculate the energetic cost of fixing carbon through the CCM. This cost is composed of three components: the cost of transport, the cost of the CBB cycle, and the cost of photorespiratory pathways recycling 2PG (Fig. 3). The per-fixation

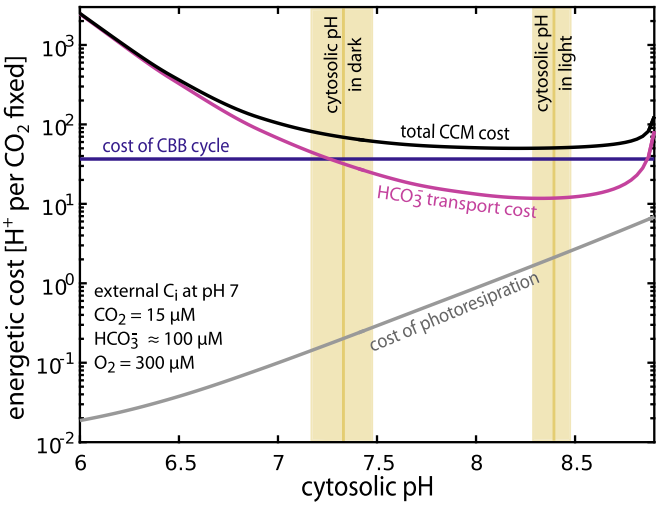

Fig. 3. Energetic costs associated with the CCM depend strongly on the cytosolic pH. The total energetic cost of concentrating CO_2 per CO_2 fixation (black) is plotted for cytosolic pH ranging from 6 to 9. The purple line denotes the cost of HCO_3^- transport and the blue line gives the per-fixation cost of the CBB cycle, which is assumed to be independent of pH. The gray line gives the cost of recycling 2PG through the C_2 photorespiratory pathway. The measured cytosolic pH of *S. elongatus* 7942 is shown as gold bars with bar width denoting the SE (*Methods*). The extracellular Ci pool was assumed to be in equilibrium with the external pH, which was fixed at 7 for this analysis.

cost of the CBB cycle is approximately constant, but the costs of transport and photorespiration depend on the pH and the efficacy of the CCM (i.e., how much carboxylation and oxygenation take place). Here, we express the cost of fixation in units of H^+ gradient dissipation— the number of H^+ transported along the concentration gradient (i.e., the fundamental currency of the electrochemical potential). Cyanobacteria convert a proton gradient into ATP by means of the F_1F_o ATP synthase, which synthesizes one ATP for every four H^+ translocated (40, 41).

Active transport of Ci is the chief energetic cost associated with the CCM. The biochemical mechanism of facilitated CO_2 uptake is not known and so we focus on the primary cyanobacterial HCO_3^- transporters, Na^+ symporters, which import one Na^+ with each HCO_3^-. In model cyanobacteria like *S. elongatus*, antiporters exchange Na^+ and H^+, and so sodium and proton gradients are interchangeable (7, 42). This allows HCO_3^- transport cost to be expressed in units of H^+ transported across the membrane per CO_2 fixed. We assume a cost of four H^+ per HCO_3^- transported (*SI Appendix*) to calculate the per-fixation cost of HCO_3^- transport shown in Fig. 2.

The cost of the CBB cycle and the C_2 photorespiratory pathway can be estimated from their known stoichiometry. We calculate the cost of the CBB cycle as ≈37 H^+ per CO_2 fixed and the cost of the C_2 pathway ≈26 H^+ per 2PG recycled (*SI Appendix*). The total cost of CO_2 fixation and 2PG recovery will depend on the relative amount of oxygenation according to the formula

$$\text{fixation and recovery cost} = \frac{(37 + 26\ R_O)}{1 - \frac{R_O}{2}},$$

where R_O is the ratio of oxygenation to carboxylation rates ($R_o = V_o/V_c$), 37 H^+ is the per-carboxylation cost of the CBB cycle, and 26 H^+ is the per-oxygenation cost of C_2 photorespiration. The cost has units of H^+ per carboxylation. This formula accounts for the fact that each turn of the C_2 cycle releases one CO_2, which must be fixed again to maintain carbon balance (*SI Appendix*). In the limit of low photorespiration, R_o approaches zero and the above formula converges to ≈37 H^+ per CO_2, the calculated cost of fixation through the CCB cycle. As the modeled CCM strongly limits oxygenation, the "fixation and recovery cost" is dominated by the cost of the CBB cycle, which is roughly constant (blue line in Fig. 3). The rate and cost of photorespiration, in contrast, is tied to the ratio of CO_2 to O_2 in the carboxysome (i.e., CCM efficacy) and so depends on pH (gray line in Fig. 3).

The projected cost of transport (purple line) falls beneath that of the CBB cycle (Fig. 3) as the cytosolic pH surpasses 7. The modeled cyanobacterial CCM approaches a total cost of ≈50 H^+ per fixation near pH 8. At pH ≈8, active transport costs about 10-fold less than the CBB cycle and, we calculate, requires <1% of cell surface area (*SI Appendix*). Notably, photorespiratory costs increase at elevated pH (Fig. 3) and oxygenation could account for as many as 2% of RuBisCO turnovers near pH 8. This might explain the absolute requirement for photorespiratory pathways in model cyanobacteria (43). Increased photorespiration can be understood as follows: CA equilibrates CO_2 with HCO_3^- in the carboxysome and increased pH favors HCO_3^- over CO_2 (*SI Appendix*, Fig. S1). As such, the carboxysomal CO_2 concentration decreases as the pH increases, increasing the O_2:CO_2 ratio and, consequently, photorespiration. So long as the pH remains beneath 8.5, the cost of photorespiration never exceeds 3% of total. Taken together, these cost calculations suggest that a cytosolic 7.5 < pH < 8.5 minimizes total energetic costs without requiring substantial photorespiratory flux. At a cytosolic pH <6.2 transport is prohibitively costly, at least an order of magnitude more so that carbon fixation itself.

***S. elongatus* Cytosolic pH is Within the Optimal Range for CCM Operation.** Increased cytosolic pH decreases the permeability of the bicarbonate pool to the cell membrane, reduces the amount of HCO_3^- transport required per CO_2 fixation, and decreases the total cost of CO_2 fixation through the CCM. Our model predicts an optimal cytosolic pH range of 7.5–8.5 to minimize the total energetic cost of fixing carbon through the CCM. To test the prediction of an optimal cytosolic pH range, we measured the cytosolic pH of light- and dark-acclimated cyanobacteria (*S. elongatus* PCC 7942) using the ratiometric pH-sensitive dye BCECF-AM (*Methods*). As shown in Fig. 3, cytosolic pH differs between dark-acclimated cells, which do not grow or fix CO_2 appreciably, and light-acclimated cells, which fix carbon and grow. Strikingly, the cytosolic pH of *S. elongatus* increases from 7.3 ± 0.2 in the dark to 8.4 ± 0.1 in the light (Fig. 3 and *SI Appendix*, Fig. S8). This is expected because the photosynthetic light reactions pump H^+ from the cytosol into the thylakoid lumen (44) and the pH values are consistent with previous measurements of cytosolic pH in cyanobacteria (45–48). The pH in the light coincides well with our prediction of an optimal cytosolic pH range for carbon-fixing cyanobacteria.

Discussion

Here, we demonstrate that CCM function is strongly dependent on pH. Most importantly, we show that Ci leakage is dominated by H_2CO_3 within the physiological pH range (*SI Appendix*). Elevated cytosolic pH increases the relative abundance of charged HCO_3^- and so reduces leakage and the energetic cost of maintaining a high cytosolic concentration of H_{total}. This mirrors heterotrophic transport strategies such as the phosphorylation of glucose after uptake, which serves to "trap" glucose in the cell. We predict an optimal cytosolic pH range of 7.5–8.5 for carbon-fixing cyanobacteria. At pH 7.7 the total energetic cost of fixing carbon through the CCM is minimized, with higher pH offering diminishing returns (Fig. 3). We experimentally verified that cyanobacteria (*S. elongatus* 7942) achieve a cytosolic pH in this range while fixing carbon (Fig. 3). Moreover, *S. elongatus* cytosolic pH in the light (during carbon fixation) is ≈8.4 and differs markedly from the pH ≈7.3 measured in dark-acclimated cells (Fig. 3).

Notably, efficient operation of the CCM depends on two crucial unknown parameters: the velocity of active HCO_3^- transport and the permeability of the carboxysome to CO_2 and HCO_3^- (14). These parameters are interdependent: Changing the carboxysome permeability alters the HCO_3^- transport flux required to concentrate CO_2 in the carboxysome, as shown in *SI Appendix*, Fig. S6. Integrating pH into the model does not qualitatively change the interdependence of carboxysome permeability and active HCO_3^- transport. However, at pH 8, the pH-aware CCM model demands 10^2 to 10^4 times less active HCO_3^- transport than our previous model to achieve efficient CO_2 fixation (Fig. 2). We defined the optimum permeability as the value that minimizes the active HCO_3^- transport flux required to saturate RuBisCO. The optimal carboxysome permeability at pH 8 is also 30-fold lower than previously reported (3×10^{-5} instead of 10^{-3} cm/s), but carboxysome permeabilities as high as 10^{-2} cm/s can support CO_2-concentrating activity (*SI Appendix*, Fig. S6).

This updated, pH-aware model now agrees with cyanobacterial physiology in several ways. In optimal pH conditions the predicted fluxes for HCO_3^- transport, leakage, and carboxylation are all within an order of magnitude of measured values (23). In contrast to earlier models, which required >50% of the cell membrane surface for Ci transport, these fluxes demand less than 1% of cell membrane surface area (*SI Appendix*). The pH-aware model also helps rationalize the distribution of Ci transport systems among cyanobacteria. Freshwater cyanobacteria, which live near neutral pH, typically have genes coding for both facilitated CO_2 uptake and energetically activated HCO_3^- transport systems. Oceanic cyanobacteria, which live at pH ≈8, typically encode only HCO_3^- transporters (23, 32). Based on our analysis of the pH-aware model, a sizable fraction of Ci can be taken up as CO_2 in a near-neutral pH

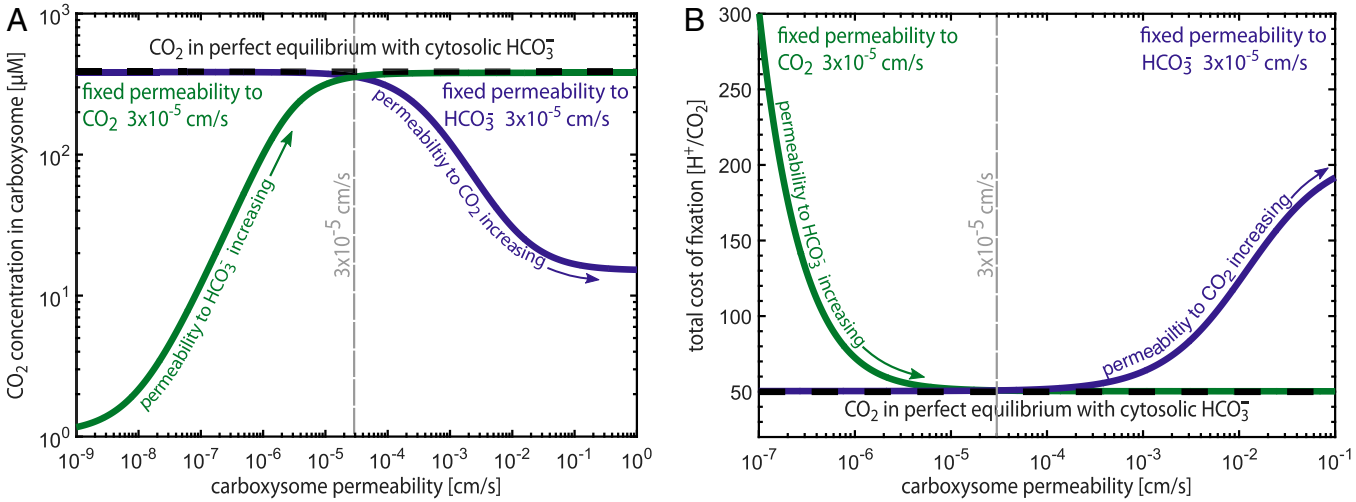

Fig. 4. A selective carboxysome would not substantially improve CCM efficiency. The CO_2 concentration in the carboxysome is maximized when it is brought into equilibrium with the cytosolic HCO_3^- pool, shown as the black dashed line in *A* and *B*. A CCM using the single optimal permeability computed through the pH-aware model (dashed gray line) achieves a carboxysomal CO_2 concentration within 5% of this maximum. Selectivity at the carboxyome shell is thought to increase HCO_3^- permeability relative to CO_2 by means of charge interactions in the pores of the carboxysome shell. Selectivity might intuitively result in greater trapping of CO_2 (tracing the purple curve toward lower permeabilities) or faster uptake of HCO_3^- (tracing the green curve toward higher permeabilities), but neither of these strategies can increase the carboxysomal CO_2 concentration above equilibrium. As shown in *B*, selectivity would not substantially reduce the total cost of fixing carbon through the CCM, which is already nearly minimized at the single optimal permeability of 3×10^{-5} cm/s. Increasing the CO_2 permeability beyond 10^{-4} cm/s, however, exponentially increases the cost of fixation due to leakage of CO_2 from the carboxysome to the cytosol.

environment like freshwater, whereas in an environment at pH 8 CO_2 uptake would contribute negligibly to the overall Ci uptake rate (*SI Appendix*, Fig. S9).

Selectivity at the Carboxysome Shell. Throughout the text, we assumed that the carboxysome is equally permeable to CO_2 and HCO_3^-. However, recent structures of carboxysome shell proteins offer a potential mechanism for differential permeability of CO_2 and HCO_3^-: The pores of shell proteins typically carry positive charge, which might increase the rate of HCO_3^- transit relative to CO_2 (12, 49). Indeed, recent experimental evidence suggests that protein compartments can be selectively permeable (50, 51). Intuitively, it seems that a very high HCO_3^- permeability and a very low CO_2 permeability would be best for the efficient operation of the CCM. Such permeabilities would maximize HCO_3^- uptake and minimize loss of CO_2, ensuring that every carbon entering the carboxysome is ultimately fixed.

We used the pH-aware model to examine this intuition. As shown in Fig. 4, selectivity does not substantially improve the performance of the CCM. Rather, we find that a low permeability for CO_2 ($<10^{-4}$ cm/s) is a critical requirement for CCM function. To explain this nonintuitive result, note that the best possible case for the CCM is that the carboxysomal CA brings the cytosolic HCO_3^- pool into perfect equilibrium with CO_2 inside the carboxysome (i.e., with negligible leakage of carboxysomal CO_2; dashed black line in Fig. 4*A*). Because no energetic coupling is known or hypothesized to exist inside the carboxysome, equilibration of cytosolic HCO_3^- with carboxysomal CO_2 would maximize the carboxysomal CO_2 concentration. Indeed, the optimal single carboxysome permeability $k_c = 3 \times 10^{-5}$ cm/s very nearly achieves this equilibrium CO_2 concentration (within 5%; gray dashed line in Fig. 4*A*).

Whereas a selective system could reduce the amount of active HCO_3^- transport required per fixation (*SI Appendix*), transport costs represent ~20% of the total cost at a cytosolic pH of 8 (Fig. 3) and so selectivity would have only a very small effect on the total cost of fixation in these conditions (<2%; gray dashed line in Fig. 4*B*). Increasing the permeability of the carboxysome to CO_2 beyond 10^{-4} cm/s, however, exponentially increases the cost of fixation irrespective of the HCO_3^- permeability (Fig. 4*B* and *SI Appendix*). As a result, we find that selectivity is not necessary to produce a functional and energetically efficient CCM and suggest that future research should focus on understanding how the carboxysome maintains a permeability barrier to CO_2 (*SI Appendix*).

A Relatively Acidic Carboxysome Would Benefit the CCM. It has been suggested that the carboxysome might maintain a pH gradient, with the cytosolic and carboxysomal pHs differing (37, 52). Altering the pH in the carboxysome would influence CCM efficiency in two ways. pH affects the equilibrium composition of Ci and the kinetics of the carboxysomal enzymes. A more acidic pH <8 would increase the equilibrium CO_2 concentration relative to the cytosol (*SI Appendix*, Fig. S1) and increase RuBisCO's maximum carboxylation rate (*SI Appendix*, Fig. S4). Indeed, because the combined action of CA and RuBisCO produces a net H^+, it may be possible for the cell to maintain a steady state where the carboxysomal pH differs from the cytosol (*SI Appendix*).

Fig. 5 shows that, within limits, a relatively acidic carboxysome would result in a higher degree of RuBisCO saturation at the same rate of cellular HCO_3^- uptake, with a carboxysomal pH ≈7 minimizing the amount of HCO_3^- uptake required to saturate RuBisCO (blue region). If the carboxysome is too acidic, however, it can deleteriously affect RuBisCO kinetics (*SI Appendix*, Fig. S4). An alkaline carboxysomal pH >8.5 would encumber the CCM on two fronts: As the pH increases, the equilibrium CO_2 concentration decreases exponentially and RuBisCO's maximum carboxylation rate vanishes (34). Furthermore, we find that a cytosolic HCO_3^- concentration beneath ≈10 mM is insufficient to saturate the carboxysomal RuBisCO (Fig. 5 and *SI Appendix*). This can be seen by calculating the CO_2 concentration that would be achieved by equilibrating 5 mM HCO_3^-, $[CO_2] = [HCO_3^-]10^{(pK_{eff}-pH)} \approx 5 \text{ mM} \times 10^{6.1-7} \approx 600$ μM, where pK_{eff} = 6.1 is the effective pK_a, between aqueous CO_2 and HCO_3^- (*SI Appendix*). The modeled RuBisCO, by contrast, has a carboxylation K_m that increases with decreasing pH, reaching ~1 mM at pH 7 (*SI Appendix*, Fig. S4), and so cannot be saturated by 5 mM cytosolic HCO_3^-. Although the absolute carboxylation K_m varies between RuBisCO forms (2), the plant enzyme displays a similar

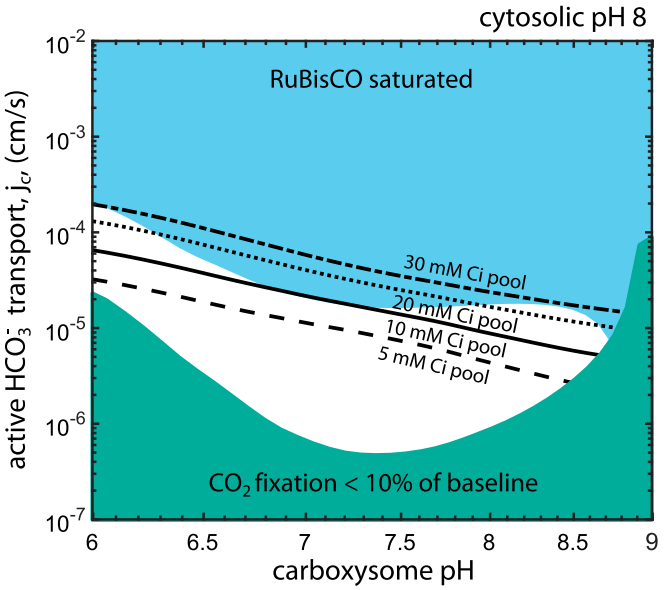

Fig. 5. A relatively acidic carboxysome would improve CCM performance. The phase space depicts the effect of varying carboxysomal pH and HCO_3^- transport on the degree of RuBisCO saturation in the carboxysome. The cytosolic pH was set to 8. The blue region denotes the portion of phase space wherein RuBisCO is saturated with CO_2. When the carboxysomal pH is relatively acidic (roughly pH 7) less HCO_3^- uptake is required to saturate RuBisCO because the equilibrium between CO_2 and HCO_3^- favors CO_2 more than at pH 8 (*SI Appendix*). Moreover, RuBisCO has an increased carboxylation k_{cat} at this pH. The minimum cytosolic HCO_3^- concentration (black lines) that allows for saturation of the carboxysomal RuBisCO is 10–20 mM, depending on RuBisCOs CO_2 affinity, which also varies with pH (*SI Appendix*). The teal region denotes the portion of phase space where the total CO_2 fixation flux is less than 10% of the flux in reference conditions (pH 8 in the cytosol and carboxysome). This region is labeled to emphasize that the fixation flux collapses at basic pH because the carboxylation k_{cat} is projected to vanish in this regime (*SI Appendix*, Fig. S4*A*).

pH dependence, with pH 7 resulting in at least twofold reduced CO_2 affinity (34, 53, 54).

Model Assumptions and Future Directions. The major insight of the pH-aware model is that the effective permeability of the membrane to H_{total} depends on the relative abundance of the species comprising H_{total} (HCO_3^-, H_2CO_3, and CO_3^{2-}) and hence on the pH and ionic strength (*SI Appendix*). The model ignores the effect of H_2CO_3 and CO_3^{2-} on all other CCM fluxes. HCO_3^- is the true substrate of CA, so it is reasonable to ignore the enzyme's interaction with other species (55). However, it is not known whether HCO_3^-, H_2CO_3, and CO_3^{2-} are equally permeable to the carboxysome. As mentioned above, pores on the carboxysome shell often carry positive charge, so it is plausible that charge would affect the rate substrates enter the carboxysome (12, 49). Direct measurement of the permeability characteristics of the carboxysome would be of great help in understanding the CCM.

We further assume throughout this work that CO_2 is the limiting substrate for RuBisCO carboxylation, that is, that the carboxylation rate does not depend on the concentration of the five-carbon carboxylation substrate ribulose-1,5-bisphosphate (RuBP). This assumption is supported by measurements of millimolar RuBP in *S. elongatus* (37), but it remains unclear how RuBP enters the carboxysome (49, 56). Similarly, we assume that O_2 enters the carboxysome quickly enough to equalize concentrations across the carboxysome shell (*SI Appendix*), that is, that the CCM is not an "oxygen-blocking mechanism."

In our analysis of the membrane permeability of H_{total}, we assumed that the permeability of H_2CO_3 is well-approximated by those of formic and acetic acids (H_2CO_2 and $H_4C_2O_2$, respectively; *SI Appendix*). Model results are particularly sensitive to our assumptions about membrane and carboxysome permeabilities (*SI Appendix*, Fig. S11), emphasizing that quantitation of these permeability values is vital to understanding the cyanobacterial CCM. We further assume the cytosolic and carboxysomal pH are equal based on the observation of fast pH equilibration across the α-carboxysome shell (52). However, it may be possible for the CCM to maintain a ΔpH across the carboxysome shell (*SI Appendix*). Although the pH-aware model suggests that a relatively acidic carboxysomal pH ≈7 would enhance CCM efficiency (Fig. 5), it is difficult to imagine how the carboxysomal pH might be measured in vivo. Finally, we assume a 30 mM concentration of cytosolic HCO_3^- based on a number of measurements (37–39), and we ignored the effect of uncatalyzed dehydration on the cytosolic HCO_3^- concentration. In the *SI Appendix* we show that the spontaneous interconversion of HCO_3^- and CO_2 has the same pH dependence as H_{total} permeability and including this reaction would result in a 15% increase in the HCO_3^- transport rate at most. As discussed above, ≈10 mM is the lowest cytosolic HCO_3^- concentration that would saturate the modeled carboxysomal RuBisCO with CO_2 (Fig. 5 and *SI Appendix*).

A long history of research into photosynthetic physiology has shown that diverse phototrophs maintain a basic pH near 8 around RuBisCO while fixing carbon. Spinach chloroplasts, which contain no CCM, maintain a pH near 7 in the dark and shift to pH ≈8 in the light (57). As such, it is unclear whether the prevailing pH is an adaptation to the CCM or the CCM adapted to the pH. Indeed, active photosynthesis requires pumping of protons into the thylakoid and so it is sensible that the pH should increase in the stroma/cytoplasm (45, 58). We simply note that these explanations are not mutually exclusive (i.e., that it is possible that a pH ≈8 results from photosynthetic proton pumping and also optimizes CCM efficiency). Many eukaryotic algae have a CCM based on a structure called the pyrenoid that is evolutionarily distinct from, but physiologically similar to, the cyanobacterial CCM (7). Similar coordinated pH shifts are also known to occur in algal chloroplasts (59). Perhaps a shift from pH ≈7 in the dark to pH ≈8 in the light reflects a coordination of chloroplast pH with the algal CCM. We hope that future investigations into pH homeostasis and intracellular fluxes of carbon-fixing organisms help refine our understanding of the inner workings of CCMs.

Methods

Modeling. The analytic equations of our previous model (14) were updated to account for the effect of pH on the composition of H_{total}, H_{total} membrane permeability, and RuBisCO and CA activity. The pH-dependent composition of H_{total} was calculated using thermodynamic potentials derived by Noor et al. (36). Permeability coefficients for CO_2, H_2CO_3, and HCO_3^- and were derived from literature values for those and similar molecules. The pH dependence of RuBisCO and CA kinetics were extracted from biochemical studies and scaled to match the carboxysomal enzymes. We further developed a mathematical framework to integrate the pH dependence of H_{total} permeability and selectivity at the carboxysome shell while preserving our capacity to solve the model analytically. In addition to the integration of detailed pH dependence, we described a carbon flux balance relation and model the energetic cost of all fluxes in the model except for facilitated CO_2 uptake. To verify the accuracy of our analytic solutions, we compared them to results produced by simulating a numerical model. The updated model is described in detail in *SI Appendix*, implemented in MATLAB and freely available at https://github.com/SavageLab/ccm/.

***S. elongatus* pH Measurement.** The intracellular pH of *S. elongatus* 7942 was measured using the ratiometric pH dye 2′,7′-bis(2-carboxyethyl)-5 (6)-carboxyfluorescein acetoxymethyl ester (BCECF-AM). The calibration curve was generated as follows. *S. elongatus* 7942 was grown to midlog phase, washed, and resuspended in BG11 media with 20 μM BCECF-AM. Cells were incubated with BCECF-AM for 30 min in the light at 30 °C and then resuspended in BG11 of defined pH containing 20 μM of the ionophore nigericin. After a 10-min incubation, four replicates of each pH condition were quickly loaded onto a 96-well plate and fluorescence was measured in a Tecan M1000 plate reader with

excitation/emission pairs 440/535 and 490/535. The 490:440 emission ratio was fit to a Boltzmann sigmoid to generate the calibration curve in *SI Appendix*, Fig. S8.

S. elongatus 7942 in midlog phase was preincubated in light or in the dark for 9 h. These cultures were washed and resuspended in their spent growth media with 20 μM BCECF-AM and incubated for 30 min at 30 °C in the light or dark as appropriate. For dark-treated cultures, all pipetting steps were carried out in a dark room with a low-intensity green LED light. Fluorescence was measured as above. Fluorescence ratios were calculated for each replicated and converted to pH values by inverting the calibration curve.

ACKNOWLEDGMENTS. We thank Arren Bar-Even, Elad Noor, Christopher Jakobson, Patrick Shih, Yinon Bar-On, Martin Jonikas, Dan Arlow, Dan Tawfik, John Raven, Grant Rotskoff, Anna Chen, Luke Oltrogge, Yoni Savir, Rosalie Lawrence, Niv Antonovsky, Sumedha Ravishankar, Jeremy Roop, and Antony Lee for fruitful discussions and helpful insight. This work was supported by a National Science Foundation Graduate Research Fellowship (to A.F.), European Research Council Grant NOVCARBFIX 646827 (to R.M.), and US Department of Energy Grant DE-SC0006394 (to D.F.S.). R.M. is the Charles and Louise Gartner Professional Chair.

1. Raven JA, Cockell CS, De La Rocha CL (2008) The evolution of inorganic carbon concentrating mechanisms in photosynthesis. *Philos Trans R Soc Lond B Biol Sci* 363(1504): 2641–2650.
2. Savir Y, Noor E, Milo R, Tlusty T (2010) Cross-species analysis traces adaptation of Rubisco toward optimality in a low-dimensional landscape. *Proc Natl Acad Sci USA* 107(8):3475–3480.
3. Tcherkez GGB, Farquhar GD, Andrews TJ (2006) Despite slow catalysis and confused substrate specificity, all ribulose bisphosphate carboxylases may be nearly perfectly optimized. *Proc Natl Acad Sci USA* 103(19):7246–7251.
4. Cleland WW, Andrews TJ, Gutteridge S, Hartman FC, Lorimer GH (1998) Mechanism of Rubisco: The carbamate as general base. *Chem Rev* 98(2): 549–562.
5. Ogren WL (1984) Photo respiration: Pathways, regulation, and modification. *Annu Rev Plant Physiol* 35:415–442.
6. Bauwe H, Hagemann M, Fernie AR (2010) Photorespiration: Players, partners and origin. *Trends Plant Sci* 15(6):330–336.
7. Kaplan A, Reinhold L (1999) CO_2 concentrating mechanisms in microorganisms. *Annu Rev Plant Physiol Plant Mol Biol* 50:539–570.
8. Rae BD, Long BM, Badger MR, Price GD (2013) Functions, compositions, and evolution of the two types of carboxysomes: Polyhedral microcompartments that facilitate CO_2 fixation in cyanobacteria and some proteobacteria. *Microbiol Mol Biol Rev* 77(3): 357–379.
9. Dou Z, et al. (2008) CO_2 fixation kinetics of Halothiobacillus neapolitanus mutant carboxysomes lacking carbonic anhydrase suggest the shell acts as a diffusional barrier for CO_2. *J Biol Chem* 283(16):10377–10384.
10. Price GD, Badger MR (1989) Expression of human carbonic anhydrase in the cyanobacterium Synechococcus PCC7942 creates a high CO(2)-requiring phenotype : Evidence for a central role for carboxysomes in the CO(2) concentrating mechanism. *Plant Physiol* 91(2):505–513.
11. Volokita M, Zenvirth D, Kaplan A, Reinhold L (1984) Nature of the inorganic carbon species actively taken up by the cyanobacterium Anabaena variabilis. *Plant Physiol* 76(3):599–602.
12. Yeates TO, Kerfeld CA, Heinhorst S, Cannon GC, Shively JM (2008) Protein-based organelles in bacteria: Carboxysomes and related microcompartments. *Nat Rev Microbiol* 6(9):681–691.
13. Magid E, Turbeck BO (1968) The rates of the spontaneous hydration of CO_2 and the reciprocal reaction in neutral aqueous solutions between 0 degrees and 38 degrees. *Biochim Biophys Acta* 165(3):515–524.
14. Mangan N, Brenner M (2014) Systems analysis of the CO_2 concentrating mechanism in cyanobacteria. *eLife* 3:e02043.
15. Fridlyand L, Kaplan A, Reinhold L (1996) Quantitative evaluation of the role of a putative CO_2-scavenging entity in the cyanobacterial CO_2-concentrating mechanism. *Biosystems* 37(3):229–238.
16. Reinhold L, Kosloff R, Kaplan A (1991) A model for inorganic carbon fluxes and photosynthesis in cyanobacterial carboxysomes. *Can J Bot* 69:984–988.
17. Reinhold L, Zviman M, Kaplan A (1987) *Progress in Photosynthesis Research* (Springer, Berlin), pp 289–296.
18. McGrath JM, Long SP (2014) Can the cyanobacterial carbon-concentrating mechanism increase photosynthesis in crop species? A theoretical analysis. *Plant Physiol* 164(4): 2247–2261.
19. Hopkinson BM, Young JN, Tansik AL, Binder BJ (2014) The minimal CO_2-concentrating mechanism of Prochlorococcus spp. MED4 is effective and efficient. *Plant Physiol* 166(4):2205–2217.
20. Robertson RN (1983) *The Lively Membranes* (Cambridge Univ Press, Cambridge, UK).
21. Gutknecht J, Bisson MA, Tosteson FC (1977) Diffusion of carbon dioxide through lipid bilayer membranes: Effects of carbonic anhydrase, bicarbonate, and unstirred layers. *J Gen Physiol* 69(6):779–794.
22. Xiang T-X, Anderson BD (1994) The relationship between permeant size and permeability in lipid bilayer membranes. *J Membr Biol* 140(2):111–122.
23. Hopkinson BM, Young JN, Tansik AL, Binder BJ (2014) The minimal CO_2-concentrating mechanism of Prochlorococcus spp. MED4 is effective and efficient. *Plant Physiol* 166(4):2205–2217.
24. Schuetz R, Zamboni N, Zampieri M, Heinemann M, Sauer U (2012) Multidimensional optimality of microbial metabolism. *Science* 336:601–604.
25. Flamholz A, Noor E, Bar-Even A, Liebermeister W, Milo R (2013) Glycolytic strategy as a tradeoff between energy yield and protein cost. *Proc Natl Acad Sci USA* 110(24): 10039–10044.
26. Basan M, et al. (2015) Overflow metabolism in *Escherichia coli* results from efficient proteome allocation. *Nature* 528:99–104.
27. Alberty RA (2003) *Thermodynamics of Biochemical Reactions* (Wiley, Hoboken, NJ), 1st Ed.
28. Martinez KA, 2nd, et al. (2012) Cytoplasmic pH response to acid stress in individual cells of Escherichia coli and Bacillus subtilis observed by fluorescence ratio imaging microscopy. *Appl Environ Microbiol* 78(10):3706–3714.
29. Valkonen M, Mojzita D, Penttilä M, Bencina M (2013) Noninvasive high-throughput single-cell analysis of the intracellular pH of Saccharomyces cerevisiae by ratiometric flow cytometry. *Appl Environ Microbiol* 79(23):7179–7187.
30. Adamczyk K, Prémont-Schwarz M, Pines D, Pines E, Nibbering ETJ (2009) Real-time observation of carbonic acid formation in aqueous solution. *Science* 326(5960): 1690–1694.
31. Walter A, Gutknecht J (1986) Permeability of small nonelectrolytes through lipid bilayer membranes. *J Membr Biol* 90(3):207–217.
32. Price GD (2011) Inorganic carbon transporters of the cyanobacterial CO_2 concentrating mechanism. *Photosynth Res* 109(1-3):47–57.
33. Price GD, Badger MR, Woodger FJ, Long BM (2008) Advances in understanding the cyanobacterial CO_2-concentrating-mechanism (CCM): Functional components, Ci transporters, diversity, genetic regulation and prospects for engineering into plants. *J Exp Bot* 59(7):1441–1461.
34. Badger MR (1980) Kinetic properties of ribulose 1,5-bisphosphate carboxylase/oxygenase from Anabaena variabilis. *Arch Biochem Biophys* 201(1):247–254.
35. Heinhorst S, et al. (2006) Characterization of the carboxysomal carbonic anhydrase CsoSCA from Halothiobacillus neapolitanus. *J Bacteriol* 188(23): 8087–8094.
36. Noor E, et al. (2012) An integrated open framework for thermodynamics of reactions that combines accuracy and coverage. *Bioinformatics* 28(15):2037–2044.
37. Whitehead L, Long BM, Price GD, Badger MR (2014) Comparing the in vivo function of α-carboxysomes and β-carboxysomes in two model cyanobacteria. *Plant Physiol* 165(1):398–411.
38. Sültemeyer D, Price GD, Yu JW, Badger MR (1995) Characterisation of carbon dioxide and bicarbonate transport during steady-state photosynthesis in the marine cyanobacterium Synechococcus strain PCC7002. *Planta* 197:597–607.
39. Woodger FJ, Badger MR, Price GD (2005) Sensing of inorganic carbon limitation in Synechococcus PCC7942 is correlated with the size of the internal inorganic carbon pool and involves oxygen. *Plant Physiol* 139(4):1959–1969.
40. Koumandou VL, Kossida S (2014) Evolution of the F0F1 ATP synthase complex in light of the patchy distribution of different bioenergetic pathways across prokaryotes. *PLOS Comput Biol* 10(9):e1003821.
41. Van Walraven HS, Strotmann H, Schwarz O, Rumberg B (1996) The H+/ATP coupling ratio of the ATP synthase from thiol-modulated chloroplasts and two cyanobacterial strains is four. *FEBS Lett* 379(3):309–313.
42. Elanskaya IV, Karandashova IV, Bogachev AV, Hagemann M (2002) Functional analysis of the Na+/H+ antiporter encoding genes of the cyanobacterium Synechocystis PCC 6803. *Biochemistry (Mosc)* 67(4):432–440.
43. Eisenhut M, et al. (2008) The photorespiratory glycolate metabolism is essential for cyanobacteria and might have been conveyed endosymbiontically to plants. *Proc Natl Acad Sci USA* 105(44):17199–17204.
44. Overmann JJ, Garcia-Pichel F (2013) The phototrophic way of life. *The Prokaryotes*, eds Rosenberg E, DeLong EF, Lory S, Stackebrandt E, Thompson F (Springer, Berlin), pp 203–257.
45. Falkner G, Horner F (1976) pH changes in the cytoplasm of the blue-green alga Anacystis nidulans caused by light-dependent proton flux into the thylakoid space. *Plant Physiol* 58(6):717–718.
46. Belkin S, Mehlhorn RJ, Packer L (1987) Proton gradients in intact cyanobacteria. *Plant Physiol* 84:25–30.
47. Peschek GA, Czerny T, Schmetterer G, Nitschmann WH (1985) Transmembrane proton electrochemical gradients in dark aerobic and anaerobic cells of the cyanobacterium (blue-green alga) Anacystis nidulans: Evidence for respiratory energy transduction in the plasma membrane. *Plant Physiol* 79(1):278–284.
48. Price GD, Badger MR (1989) Isolation and characterization of high CO(2)-requiring-mutants of the cyanobacterium Synechococcus PCC7942: Two phenotypes that accumulate inorganic carbon but are apparently unable to generate CO(2) within the carboxysome. *Plant Physiol* 91(2):514–525.
49. Kinney JN, Axen SD, Kerfeld CA (2011) Comparative analysis of carboxysome shell proteins. *Photosynth Res* 109(1–3):21–32.
50. Chowdhury C, et al. (2015) Selective molecular transport through the protein shell of a bacterial microcompartment organelle. *Proc Natl Acad Sci USA* 112(10): 2990–2995.
51. Glasgow JE, Asensio MA, Jakobson CM, Francis MB, Tullman-Ercek D (2015) Influence of electrostatics on small molecule flux through a protein nanoreactor. *ACS Synth Biol* 4(9):1011–1019.
52. Menon BB, Heinhorst S, Shively JM, Cannon GC (2010) The carboxysome shell is permeable to protons. *J Bacteriol* 192(22):5881–5886.

53. Bowes G, Ogren WL, Hageman RH (1975) pH dependence of the Km (CO2) of ribulose 1,5-diphosphate carboxylase. *Plant Physiol* 56(5):630–633.
54. Servaites JC (1977) pH dependence of photosynthesis and photorespiration in soybean leaf cells. *Plant Physiol* 60(5):693–696.
55. Berg JM, Tymoczko JL, Stryer L (2002) *Biochemistry* (Freeman, New York), 5th Ed.
56. Cai F, et al. (2013) The structure of CcmP, a tandem bacterial microcompartment domain protein from the β-carboxysome, forms a subcompartment within a microcompartment. *J Biol Chem* 288(22):16055–16063.
57. Werdan K, Heldt HW, Milovancev M (1975) The role of pH in the regulation of carbon fixation in the chloroplast stroma. Studies on CO2 fixation in the light and dark. *Biochim Biophys Acta* 396:276–292.
58. Heldt HW, Werdan K, Milovancev M, Geller G (1973) Alkalization of the chloroplast stroma caused by light-dependent proton flux into the thylakoid space. *Biochim Biophys Acta* 314:224–241.
59. Braun FJ, Hegemann P (1999) Direct measurement of cytosolic calcium and pH in living Chlamydomonas reinhardtii cells. *Eur J Cell Biol* 78(3):199–208.